APPLIED GEOPHYSICS, Vol.15, No.2 (June 2018), P. 188–196, 12 Figures.
DOI:10.1007/s11770-018-0683-8

Velocity dispersion and fluid substitution in sandstone under partially saturated conditions*

Ma Xiao-Yi♦[1], Wang Shang-Xu[1], Zhao Jian-Guo[1], Yin Han-Jun[1], and Zhao Li-Ming[1]

Abstract: The elastic moduli of four sandstone samples are measured at seismic (2−2000 Hz) and ultrasonic (1 MHz) frequencies and water- and glycerin-saturated conditions. We observe that the high-permeability samples under partially water-saturated conditions and the low-permeability samples under partially glycerin-saturated conditions show little dispersion at low frequencies (2−2000 Hz). However, the high-permeability samples under partially glycerin-saturated conditions and the low-permeability samples under partially water-saturated conditions produce strong dispersion in the same frequency range (2−2000 Hz). This suggests that fluid mobility largely controls the pore-fluid movement and pore pressure in a porous medium. High fluid mobility facilitates pore-pressure equilibration either between pores or between heterogeneous regions, resulting in a low-frequency domain where the Gassmann equations are valid. In contrast, low fluid mobility produces pressure gradients even at seismic frequencies, and thus dispersion. The latter shows a systematic shift to lower frequencies with decreasing mobility. Sandstone samples showed variations in V_p as a function of fluid saturation. We explore the applicability of the Gassmann model on sandstone rocks. Two theoretical bounds for the P-velocity are known, the Gassmann–Wood and Gassmann–Hill limits. The observations confirm the effect of wave-induced flow on the transition from the Gassmann–Wood to the Gassmann–Hill limit. With decreasing fluid mobility, the P-velocity at 2–2000 Hz moves from the Gassmann–Wood boundary to the Gassmann–Hill boundary. In addition,, we investigate the mechanisms responsible for this transition.
Keywords: Sandstone, saturation, P-wave, dispersion, Gassmann, fluid substitution

Introduction

Wave dispersion and attenuation at seismic frequencies are of importance to rock physics. Variations in reservoir seismic properties are related to fluid changes. Many theoretical models have been developed to predict and account for the fluid-related attenuation of acoustic waves and the frequency dispersion of the elastic moduli of porous rocks (Mavko et al., 2009; Müller et al., 2010). The primary mechanisms are particle–fluid inertia and viscous coupling (Biot, 1956), patch saturation (White, 1975; Dutta and Ode, 1979), as well as squirt or local flow (Mavko and Jizba, 1991).

Manuscript received by the Editor March 23, 2018; revised manuscript received June 29, 2018.
*This work was supported by 973 Program “Fundamental Study on the Geophysical Prospecting of the Deep-layered Oil and Gas Reservoirs” (No. 2013CB228600).
1. State Key Laboratory of Petroleum Resources and Prospecting, China University of Petroleum (Beijing), Beijing 102249, China.
♦Corresponding author: Ma Xiao-Yi (Email: ma_xiaoyi@sina.com)

However, these theoretical models remain unconstrained by experimental data owing to the scarcity of laboratory data, especially partial saturation experiments at seismic frequencies.

In the narrow frequency band used in seismic exploration, the widely used Gassmann equation is not solved for sandstone with pore fluid, especially in partial saturation conditions. Mikhaltsevitch et al. (2014) found that low-permeability sandstones show obvious modulus dispersion and significant extensional attenuation at seismic frequencies that cannot be accounted for by the Gassmann theory. However, the seismic frequency laboratory data are relatively sparse. Batzle et al. (2006) studied the attenuation and dispersion of saturated rocks at 5 Hz to 800 kHz and described the dispersion and attenuation mechanisms; furthermore, they demonstrated that the Gassmann theory, which assumes relaxed fluid pore pressures, cannot predict the velocity variations in rocks saturated with high-viscosity fluids even at seismic frequencies. For sandstones, especially of high porosity, fluid mobility is high and pore pressure is at equilibrium at low frequencies in agreement with the Gassmann model. At any frequency, if fluid mobility is sufficiently low, pore pressure is out of equilibrium and at high seismic frequencies Gassmann theory is not applicable.

In this study, we use four sandstone samples and obtain their properties under water- and glycerin-saturated conditions by using a multi-frequency system. The main objective is to investigate the elastic properties of fluid-saturated sandstones with variable fluid mobility at seismic to ultrasonic frequencies. Finally, we compare the measured V_p moduli to the Gassmann–Wood and Gassmann–Hill model predictions. We focus on the relation between dispersion and fluid mobility at seismic and ultrasonic frequencies. The sandstone samples are from different depths but from the same well. The specimens have different mineralogy, porosity, and permeability.

Methodology

We investigated the elastic properties of fluid-saturated rocks at seismic to ultrasonic frequencies (Wang et al., 2012; Zhao et al., 2013; Zhao et al., 2015). The experimental setup was developed by the Physical Laboratory, China University of Petroleum (Beijing). High-frequency (HF) measurements are based on the ultrasonic pulse transmission method, where P- and S-wave ultrasonic transducers are placed in the upper and lower ends of a rock sample to obtain the wave propagation time (see Figure 1a). Low-frequency (LF) measurements are based on the stress–strain method, where strain gauges are used. Typical strain signals are shown in Figure 1b. As a result, both compressional and shear properties are obtained simultaneously at about 2 Hz to 1 MHz. The length of the samples was about 3–7 cm. The experiments were conducted in a container with nitrogen gas and heating bath thermostats. The confining pressure was up to 40 MPa and the temperature between 30 °C and 120 °C.

At a given effective pressure, the stress on the sample is estimated based on the strain measured at the reference aluminum standard ε_{al} and the known aluminum Young's modulus E_{al}. Thus, the Young's modulus E of the sample is calculated from the ratio of the strain amplitude between the axial gauges on the rock ε_{ax} and aluminum

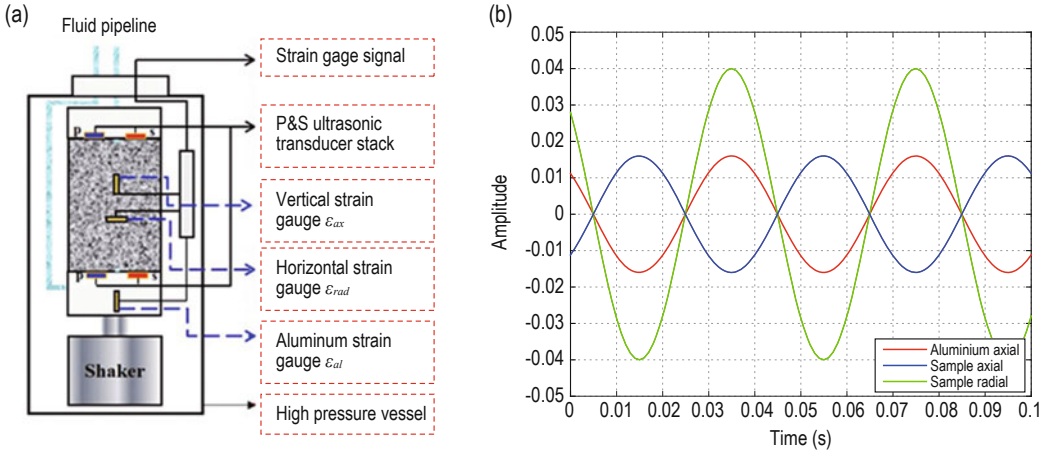

Fig.1 Multifrequency experimental setup.

(a) Schematic of the setup for measuring the elastic properties at seismic and ultrasonic frequencies with strain gauges and transducers; (b) typical responses of the extensional and axial strain gauges on a test sample and aluminum standard.

ε_{al} (Batzle, 2006)

$$E = \frac{\varepsilon_{al} E_{al}}{\varepsilon_{ax}}, \quad (1)$$

The Poisson's ratio v of the sample is

$$v = -\frac{\varepsilon_{rad}}{\varepsilon_{ax}}. \quad (2)$$

Under the assumption of isotropy and homogeneity, any two independently measured elastic properties can describe the rock elasticity. As a result, the LF compressional velocity (Vp_{LF}) and shear velocity (Vs_{LF}) are derived from the measured E and v for known rock density ρ

$$Vp_{LF} = \sqrt{\frac{E(1-v)}{(1-2v)(1+v)\rho}}, \; Vs_{LF} = \sqrt{\frac{E}{2(1+v)\rho}}. \quad (3)$$

Batzle et al. (2006) introduced the concept of fluid mobility to describe the type of pore fluids moving through a rock. Fluid mobility M is

$$M = \frac{k}{\eta}, \quad (4)$$

where k is the permeability and η is the viscosity. In the experiments, we consider and vary these two parameters. In general, for single relaxation, where pore fluids oscillate uniformly, the compressional velocity or bulk modulus will show sigmoidal increase with increasing frequency. This is shown in Figure 2.

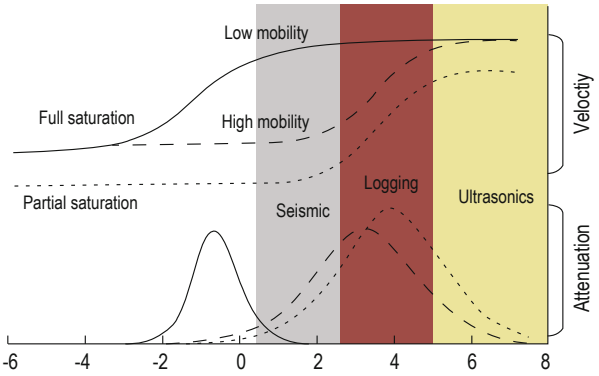

Fig.2 Schematic of the velocity dispersion and attenuation (modified after Batzle et al., 2006)

Sample description

We used sandstone samples from two different drill-cores from the same well and from depths of 2970.55 m and 3595.83 m below sea level. The well is in the Jidong oilfield, north of the Bohai Sea Bay, China. The samples from the same drill-core have very similar mineralogy and physical properties (Figure 3, and Tables 1 and 2). Thus, in the experiment, one sample is saturated with water and the other with glycerin. The observed dispersion is due to the different fluids. The samples have porosity of 16.33−21.17%, permeability of 8.34 −116.26 mD, and grain density of 2.064−2.211 g/cm^3, as given in Table 1. The samples are cylindrical, 38.2 mm in diameter and 60.3 mm to 70.3 mm in length. In Table 1, we summarize the physical characteristics of the samples. The porosity and permeability are measured using standard helium porosimetry and air permeability equipment at atmospheric pressure.

Table 1 Dimensions and physical properties of the sandstone samples

Sample	Diameter (mm)	Length (mm)	Grain density (g·cm^{-3})	Porosity	Permeability (m·D)	Depth (m)
S_1	38.2	61.8	2.084	20.54%	116.267	2970.55
S_2	38.2	60.3	2.064	21.17%	115.876	2970.55
S_3	38.2	70.3	2.211	16.33%	8.73	3595.83
S_4	38.2	69.5	2.191	17.32%	8.34	3595.83

Table 2 Lithology data for the sandstone samples

Sample	Clay mineral (%)	Quartz (%)	*K*-feldspar (%)	Plagioclase (%)	Dolomite (%)
S_1	5.8	33.8	8.3	41.4	10.7
S_2	5.9	33.5	8.1	41.7	10.8
S_3	14.1	49.7	13.3	22.9	0
S_4	14.3	50.1	13.1	22.5	0

Figure 4 shows thin sections of the sandstones. The cores have experienced mechanical compaction, pressure solution, cementation, and dissolution during diagenesis. Samples S_1 and S_2 contain dolomite, whereas samples S_3 and S_4 do not. Dolomitization is evident from the high porosity and high permeability. The mineral composition of the sandstone samples from X-ray diffraction is given Table 2.

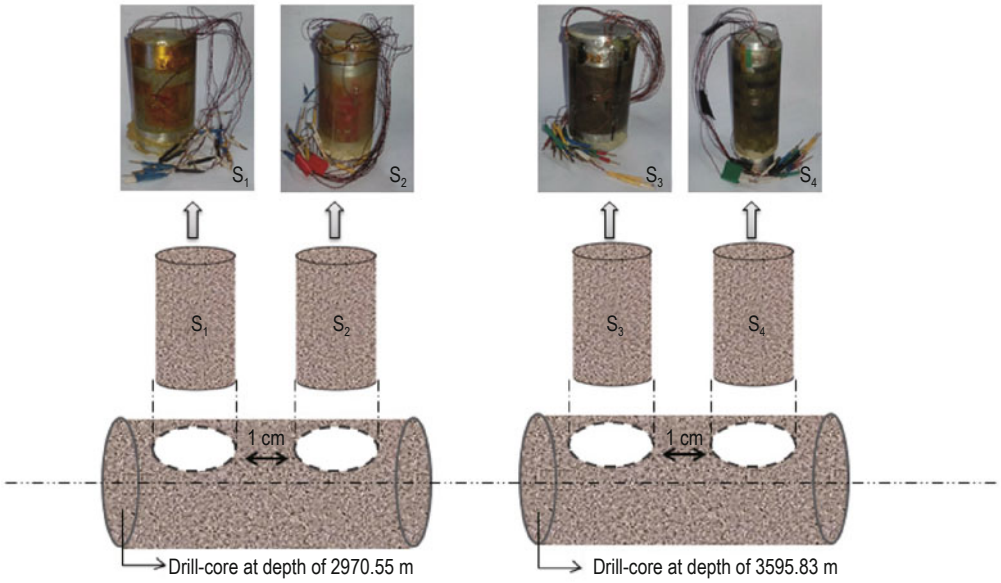

Fig.3 Sandstone samples.

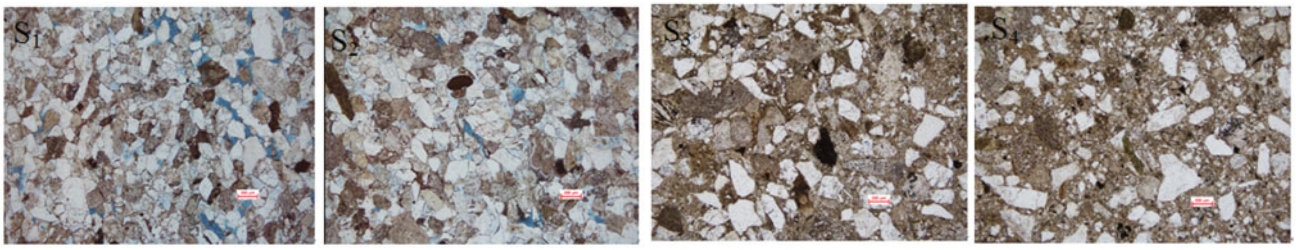

Fig.4 Thin sections of the sandstone samples.

Experimental procedure and results

We divided the four samples into two groups. One group consists of S_1 and S_2 and the other of S_3 and S_4. All samples were tested at seismic (2−2000 Hz) and ultrasonic frequencies (1 MHz), however, the fluid in the samples is different. In each group, one sample was water-saturated and the other was glycerin-saturated (Table 3). The degree of saturation is determined by the pore volume and the volume of the injected fluid. The pore volume is derived by the sample volume and porosity. The volume of the injected fluid is accurately controlled by a Teledyne ISCO pump. All testing procedures were carried out at room temperature (23 ± 2 °C) and humidity (65 ± 2% RH).

In S_1, we measured and compared the elastic moduli (Young's modulus, Poisson's ratio, bulk modulus, and shear modulus) under different water-saturated conditions. Figure 5a shows that the Young's modulus hardly changed at low frequency and dry conditions (red line). With increasing degree of saturation, Young's modulus first decreased and then increased. Figure 5b shows that Poisson's ratio increases with increasing saturation, reaching 0.27. Figure 5c shows that the bulk modulus variation is very small under unsaturated conditions but high in 100% water saturation. Shear modulus decreases slowly with increasing saturation, as shown in Figure 5d. Because the permeability is high and the water viscosity is low, the pore fluid is uniformly distributed in the sample at low frequency. The experimental data for bulk modulus and shear modulus agree with the Gassmann–Wood equation, as shown in Figure 6. During the experiment, the samples are a two-phase (gas and water) medium. Based on the Gassmann equation, the effective modulus of the pore

Table 3 Experimental conditions

Sample	Temperature (°C)	Humidity (%RH)	Injected fluid	Viscosity (cP)
S_1	23	65	Water	1.0087
S_2	23	65	Glycerin	1410
S_3	23	65	Water	1.0087
S_4	23	65	Glycerin	1410

fluid is determined by the minimum fluid component; namely, the modulus of the pore fluid is approximately equal to the modulus of the gas. Only at very high degree of saturation, the modulus of the pore fluid is equal to the modulus of the fluid. However, the bulk density of the rock increases with increasing saturation and the compressional wave velocity significantly decreases and then suddenly increases (Figure 5e). Figure 5e also shows that the variation in velocity with saturation at low frequency (2−2000 Hz) is not consistent with the ultrasonic (1 MHz) data. V_p at ultrasonic frequencies increases with increasing saturation. This implies that the dispersion effect of the mesoscale fluid flow is dominant in ultrasonic frequency. When the frequency of the pulse wave is higher, the pore pressure owing to the pulse wave is in nonrelaxation state and the rock skeleton hardens. This explains the higher V_p at ultrasonic frequency than that at low frequencies.

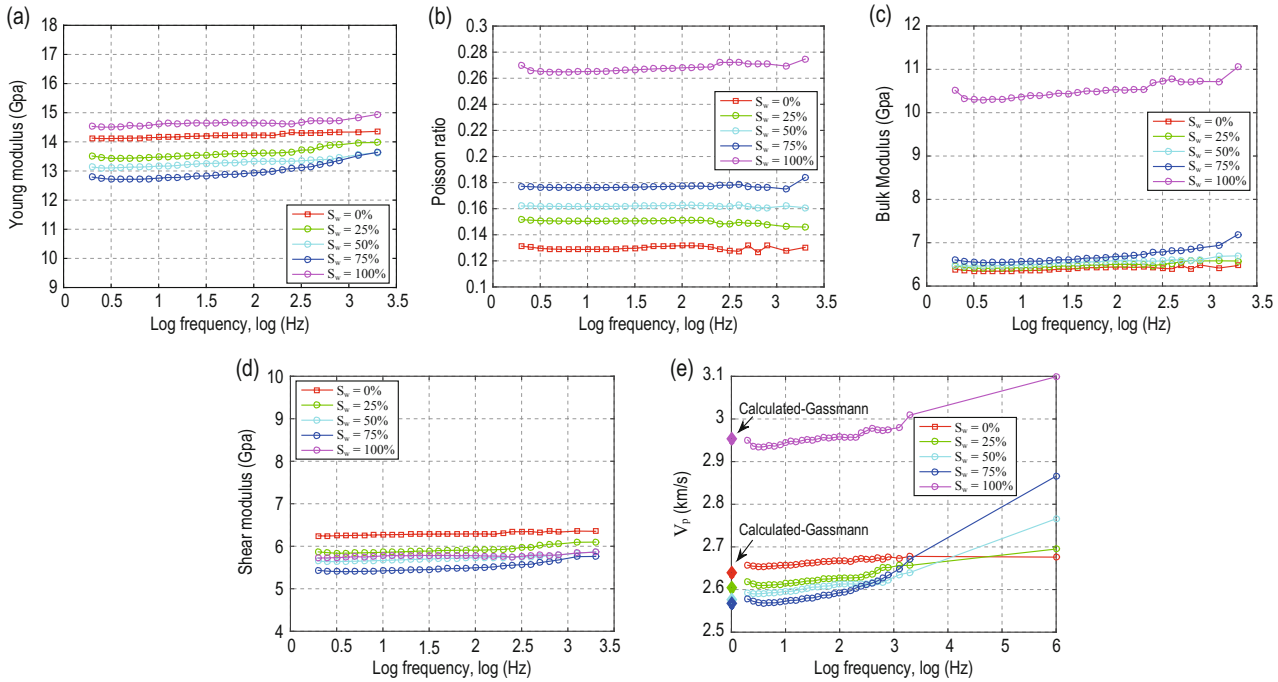

Fig.5 Elastic parameters and P-wave velocity in S_1 as a function of frequency at different water-saturated conditions.
(a) Measured Young's modulus; (b) measured Poisson's ratio; (c) measured bulk modulus; (d) measured shear modulus; (e) measured V_p and estimated velocity using the Gassmann equation.

In porous rocks with elastically homogeneous matrix and inhomogeneities owing to spatial variations in the fluid properties, two theoretical bounds for the P-velocity are known (Mavko and Mukerji, 1998). In the static or low-frequency limit, the bulk modulus of the rock is defined by the Gassmann equation and the fluid bulk modulus by the Wood equation, i.e., the saturation-weighted harmonic average of the bulk moduli of fluids. The Gassmann–Wood bound is valid when the characteristic patch size is small compared to the fluid diffusion length. The diffusion length is primarily controlled by rock permeability, fluid viscosity, and wave frequency. In the no-flow or high-frequency limit, the effective P-wave modulus can be obtained by the Hill equation, i.e., the saturation-weighted harmonic average of the P-wave moduli. The Gassmann–Wood and Gassmann–Hill bounds are the low- and high-frequency limits, respectively (Maxim et al., 2009). Figure 6 shows

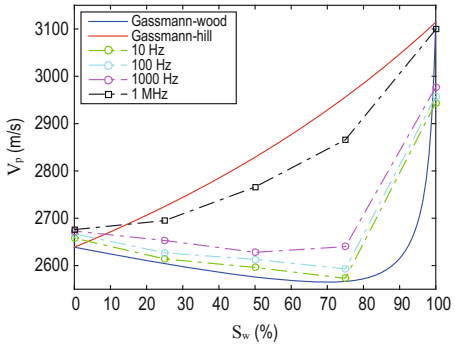

Fig.6 Measured and estimated P-wave velocities in S_1 as a function of water saturation. Seismic frequency (green and light blue), logging frequency (purple), and ultrasonic (black) data are measured. The Gassmann–Wood (GW) and Gassmann–Hill (GH) bounds are shown in blue and red, respectively.

the P-wave velocity at different frequencies. In the low-frequency (2−2000 Hz) range, the P-wave velocities are in line with the GW boundary and increase with frequency. In the ultrasonic frequency band (1 MHz), the data mimic the GH boundary.

Then, we tested sample S_2. The experimental procedure is the same but the injected fluid is glycerin. The measured V_p at different frequency bands as a function of glycerin saturation is shown in Figure 7. The compressional wave velocity variation with saturation is not consistent with the test results for S_1. The viscosity of glycerin is far higher than that of water, therefore the fluid mobility in S_2 is lower than that in S_1 based on equation 4. We observe strong dispersion well within the seismic band at relatively lower fluid mobility. This means that S_1 falls in the low-frequency regime, whereas the velocity dispersion in S_2 shifts to low frequency. In other words，lowering the fluid mobility increases the relaxation time needed for fluid equilibration and consequently the dispersion frequency is reduced.

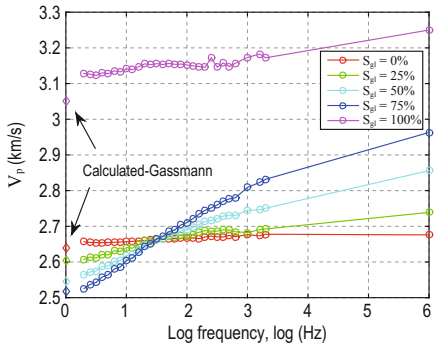

Fig.7 Measured and estimated V_p using the Gassmann equation in S_2 as a function of frequency at different glycerin saturation levels.

Next, we tested the S_3 and S_4 samples. The experimental procedure is the same but water injection is applied to S_3 and glycerin to S_4. In S_3 and S_4, permeability is lower than S_1 and S_2 and thus the mobility is lower. The results are shown in Figure 8, where the P-wave velocity data show frequency dispersion in S_3 but not in S_4. This is opposite to the data for S_1 (water-saturated) and S_2 (glycerin-saturated). The reduction in mobility decreases the dispersion and lowers the frequency. Eventually, S_4 enters the high-frequency regime and the dispersion is below 10 Hz.

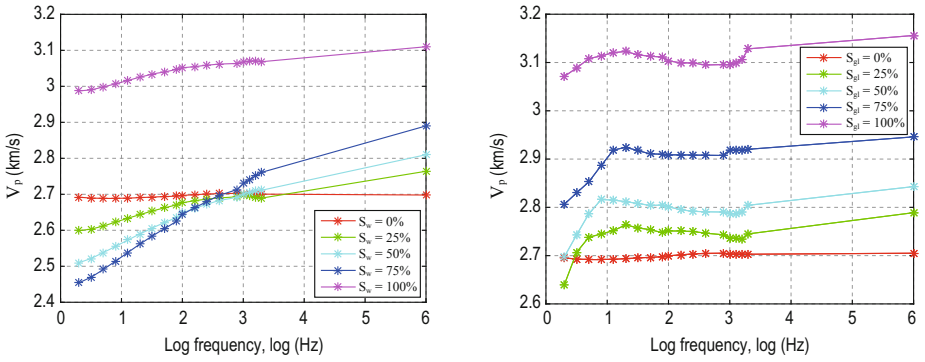

(a) S_3 (b) S_4

Fig.8 Measured V_p as a function of frequency at different degrees of saturation.

The Gassmann fluid substitution

We use the Gassmann–Wood and Gassmann–Hill models to calculate the water- and glycerin-saturated V_p and then compare them to the measured V_p. The experimental setup lets us acquire data when the fluid is at isothermal equilibrium. The bulk modulus of water is 2.25 GPa and 4.32 GPa for glycerin.

Figure 9a compares the V_p calculated using the Gassmann–Wood model and the measured V_p for the water-saturated sandstone (S_1) at 100 Hz. The Gassmann –Wood model correctly predicts the observed water-saturated V_p in the S_1 specimen, except at full saturation. The pore pressure is the equilibrium pore pressure and this is achieved at seismic frequencies or lower, where the fluid has enough time to reach relaxation or approach equilibrium. At full saturation, the viscosity of water is high and consequently the mobility and the permeability is low. Squirt flow leads to large differences between measured and theoretically predicted values. In Figure 9b, at 1 MHz, the V_p as a function of the degree of water saturation are predicted by the Gassmann–Hill model. At high frequency, the P-wave velocity is obtained by using Hill's equation.

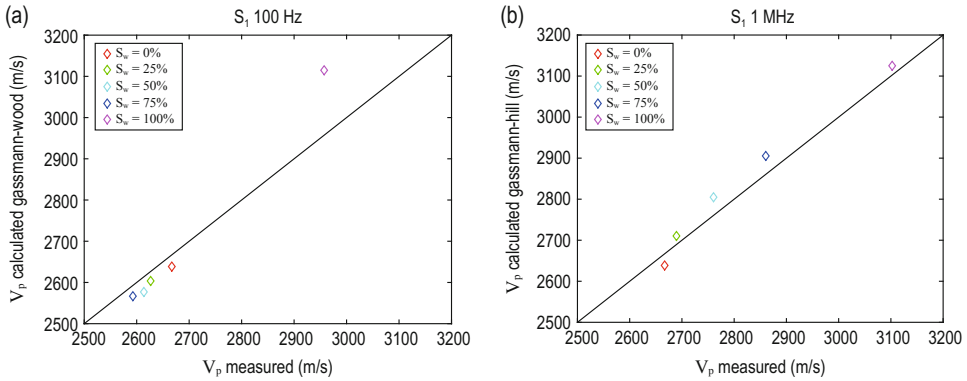

Fig.9 Water-saturated V_p, measured and estimated with the Gassmann model at 100 Hz and 1 MHz in S_1.
(a) Gassmann–Wood model at 100 Hz; (b) Gassmann–Hill model at 1 MHz.

In Figures 10a and 10b, at 100 Hz, the predicted and measured V_p do not agree. In the glycerin-saturated sandstone (S_2), the P-wave velocity increases at high frequencies. The pore pressure is not the equilibrium pore pressure because the fluid did not have time to reach relaxation or approach equilibrium. However, the relaxation time also depends on the fluid viscosity and density. The V_p is not predicted at 100 Hz by both models but it is well predicted at 1 MHz with the Gassmann–Hill (Figure 10c). The properties of samples S_1 and S_2 properties are basically the same. The injection of glycerin into sample S_2 increases the fluid viscosity by three orders of magnitude (Table 3). In Figures 5 and 7, the ultrasonic velocities show little change and only dispersion occurs at the seismic band (Figure 7). The dispersion shifts to lower frequencies with increasing viscosity. Furthermore, the glycerin-saturated sandstone is characterized by frequency dispersion, which reflects the physics of the wave dispersion and the local fluid flow.

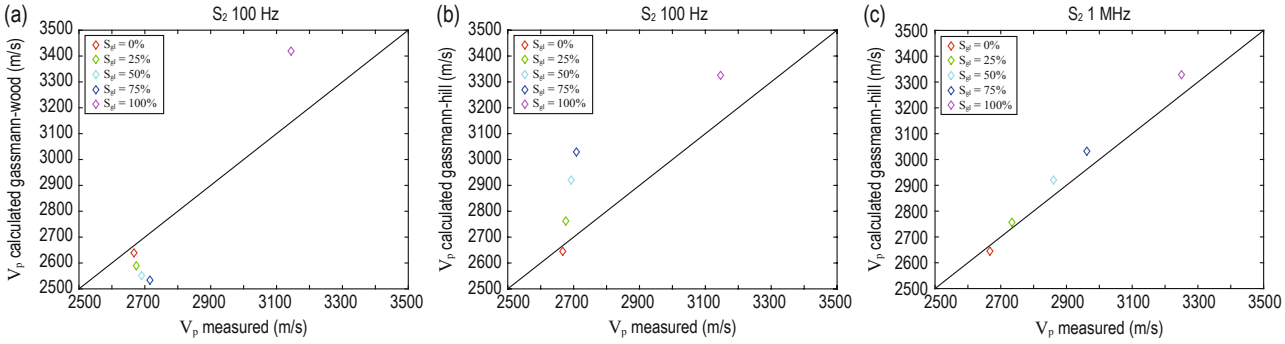

Fig.10 Glycerin-saturated V_p, measured and estimated with the Gassmann model at 100 Hz and 1 MHz in S_2.
(a) Gassmann–Wood' model at 100 Hz; (b) Gassmann–Hill model at 100 Hz; (c) Gassmann–Hill model at 1 MHz.

In the S_3 sample, the calculated with the Gassmann model and measured V_p at 100 Hz and 1 MHz are compared in Figure 11. The properties of S_3 are different from those of S_1 and S_2. Water is injected into sample S_3. At 1 MHz, test and predicted data match but not at 100 Hz. This agrees with the data for S_2. We use the Gassmann –Wood model at different degrees of water saturation at 100 Hz to predict the V_p. The test data are underestimated at any degree of saturation by the Gassmann–Wood model (Figure 11a). We use the Gassmann–Hill model at various degrees of water saturation and 100 Hz to calculate the V_p. In fact, the model overestimates the test data (Figure 11b). The Gassmann–Hill model correctly predicts the observed water-saturated V_p in S_3 at 1 MHz (Figure 11c). When saturated with water, the S_1 data show no obvious dispersion (Figure 5e), whereas the S_3 data show strong dispersion at the seismic frequency band (Figure 8a). Under water saturation, the permeability decreases and dispersion increases at the seismic frequency band. The S_1 data reflect the high permeability and high fluid mobility at the low-frequency domain. Based on Table 1, the S_3 permeability is lower than that of S_1. Most importantly, the dispersion systematically shifts to lower frequencies with decreasing permeability.

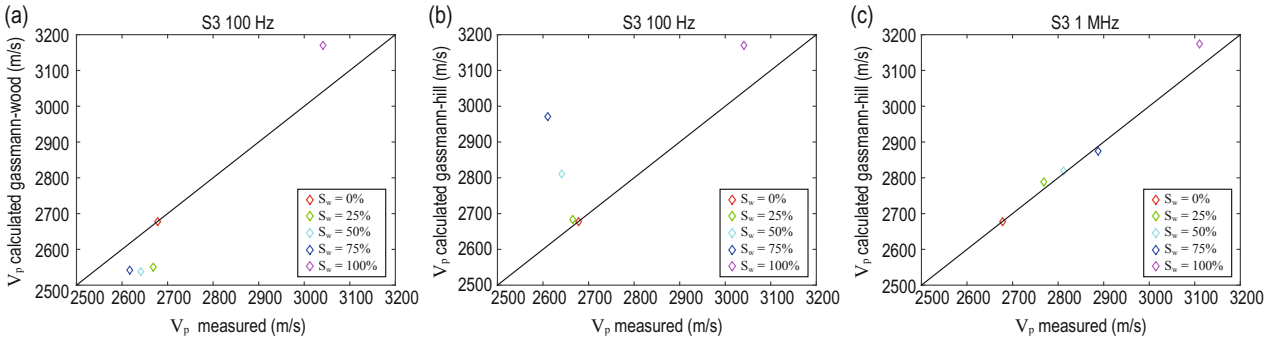

Fig.11 Water-saturated V_p, measured and estimated with the Gassmann model at 100 Hz and 1 MHz for S_3.
(a) Gassmann–Wood model at 100 Hz; (b) Gassmann–Hill model at 100 Hz; (c) Gassmann–Hill model at 1 MHz.

In glycerin-saturated S4, V_p is underestimated at 100 Hz by the Gassmann–Wood model (Figure 12a) but well predicted at 100 Hz and 1 MHz by the Gassmann–Hill model (Figures 12b and 12c). This is largely attributed to the high viscosity of the fluid and the low permeability of the rock. The ratio of rock permeability to fluid viscosity is the fluid mobility, Thus, S_4 has low fluid mobility and the rock falls in the high-frequency regime. This implies that for these rock samples, the seismic, sonic logging, and ultrasonic measurements may yield consistent velocity values. However, V_p dispersion is seen at low frequencies, below 10 Hz. Thus, the Gassmann–Hill model better fits the S_4 data at seismic and ultrasonic frequencies.

The S_1, S_2, S_3, and S_4 water- or glycerin-saturated V_p data are well predicted by the Gassmann–Hill model at ultrasonic frequencies. The Gassmann–Wood model correctly predicts the S_1 test data at low frequencies. The Gassmann–Wood and Gassmann–Hill models cannot predict the S_2 and S_3 data at low frequencies. The S_4 sample is characterized by very low permeability and high viscosity, and thus low fluid mobility. The sample falls into the high-frequency regime. This implies that the seismic and ultrasonic measurements have consistent velocity values. The Gassmann–Hill model is well suited for predicting the S_4 data at seismic and ultrasonic frequencies but further experimentation and data are needed to prove it.

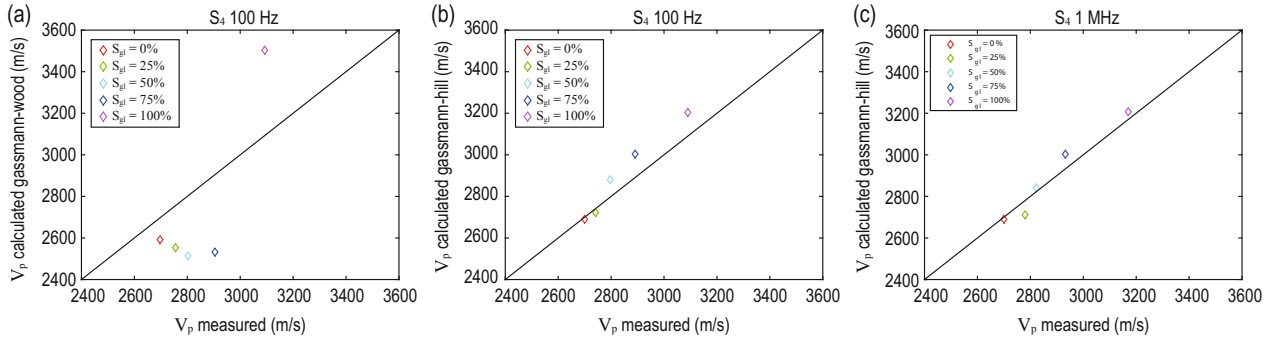

Fig.12 Glycerin -saturated V_p, measured and estimated with the Gassmann model at 100 Hz and 1 MHz in S_4.
(a) Gassmann–Wood model at 100 Hz; (b) Gassmann–Hill model at 100 Hz; (c) Gassmann–Hill model at 1 MHz.

Conclusions

We investigate the P-wave velocity dispersion under different degrees of fluid saturation and fluids and frequencies. The data demonstrate that dispersion is significant and strongly affected by fluid mobility. We also observe that it systematically shifts to lower frequencies with decreasing fluid mobility, increasing viscosity, or decreasing permeability. In all four samples, the Gassmann–Hill model well predicts the water- and glycerin-saturated V_p at ultrasonic frequencies and only the S_1 data at seismic frequency. The measured and model V_p do not agree in the S_2 and S_3 samples. The Gassmann–Hill model is well suited for S_4 at seismic and ultrasonic frequencies. The V_p data in sandstone show significant dispersion, which affects the applicability of the Gassmann model for fluid substitution at seismic frequencies. Because of the differences in mineralogy, porosity, and permeability among the sandstone

specimens, we cannot extent the conclusions to all reservoir sandstones.

Generally, the permeability of rock and viscosity of fluid span several orders of magnitude; mobility also varies by several orders of magnitude. The examined sandstones have high porosity and thus high permeability, and fall in the low-frequency regime. This allows to observe the dispersion shift to low frequencies.

References

Adam, L., and Otheim, T., 2013, Elastic laboratory measurements and modeling of saturated basalts: Journal of Geophysical Research: Solid Earth, **118**, 840–851.

Adelinet, M., Fortin, J., Guéguen Y., Schubnel A., and Geoffroy, L., 2010, Frequency and fluid effects on elastic properties of basalt: Experimental investigations: Geophysical Research Letters, **37**, L02303.

Batzle, M. L., Han, D., and Hofmann, R., 2006, Fluid mobility and frequency-dependent seismic velocity–Direct measurements: Geophysics, **71**(1), N1–N9.

Berryman, J. G., and Wang H. F., 2000, Elastic wave propagation and attenuation in a double-porosity, dual-permeability medium: International Journal of Rock Mechanics and Mineral Science, **37**, 63–78.

Biot, M. A., 1956, Theory of propagation of elastic waves in a fluid-saturated porous solid: II–Higher frequency range: Journal of the Acoustic Society of America, **28**, 179–191.

David, E. C., and Zimmerman, R. W., 2012, Pore structure model for elastic wave velocities in fluid-saturated sandstones: Journal of Geophysical Research, **117**, B07210.

Deng, J., Zhou, H., Wang, H., Zhao, J., and Wang, S., 2015, The influence of pore structure in reservoir sandstone on dispersion properties of elastic waves: Chinese Journal of Geophysics, **58**, 3389–3400.

Dutta, N. C., and Ode, H., 1979, Attenuation and dispersion of compressional waves in fluid-filled porous rocks with partial gas saturation White model: Part II: Results: Geophysics, **44**, 1789–1805.

Gary, M., and Tapan, M., 1998, Bounds on low-frequency seismic velocities in partially saturated rocks: Geophysics, **63**, 918–924.

Lucet, N., Rasolofosaon, P. N. J., and Zinszner, 1991, Sonic properties of rocks under confining pressure using the resonant bar technique: J. Acoust. Soc. Am., **89**(3), 980–990.

Mavko, G., and Jizba, D., 1991, Estimating grain-scale fluid defects on velocity dispersion in rocks: Geophysics, **56**, 1940–1949.

Mavko, G., Mukerji, T., and Dvorkin, J., 2009, The rock physics handbook: Tools for seismic analysis of porous media: Cambridge University Press.

Maxim, L., and Julianna, T. -S., 2009, Direct laboratory observation of patchy saturation and its effects on ultrasonic velocities: The Leading Edge, 24–27.

Mikhaltsevitch, V., Lebedev, M., and Gurevich, B., 2014, A laboratory study of low-frequency wave dispersion and attenuation in water-saturated sandstones: The Leading Edge, **33**, 616–622.

Müller, T. M., Gurevich, B., and Lebedev, M., 2010, Seismic wave attenuation and dispersion resulting from wave-induced flow in porous rocks—A review: Geophysics, **75**(5), 75A–147A.

Pimienta, L., Fortin J., and Guéguen, Y., 2015a, Bulk modulus dispersion and attenuation in sandstones: Geophysics, **80**(2), D111–D127.

Spencer, J. W., and Shine, J., 2016, Seismic wave attenuation and modulus dispersion in sandstones: Geophysics, **81**(3), D219–D239.

Wang, S. X., Zhao, J. G., Li, Z. H., et al., 2012, Differential Acoustic Resonance Spectroscopy for the acoustic measurement of small and irregular samples in the low frequency range: Journal of Geophysical Research, **117**(B6), B06203.

White, J. E., 1975, Computed seismic speeds and attenuation in rocks with partial gas saturation: Geophysics, **40**, 224–232.

Yin, H., Wang, S., Zhao, J., Ma, X., Zhao, L., and Cui, Y., 2016, A laboratory study of dispersion and pressure effects in partially saturated tight sandstone at seismic frequencies: 86th Annual International Meeting, SEG, Expanded Abstracts, 3236–3240.

Zhao, J., Tang, G. Y., Deng, J. X., Tong, X. L., and Wang, S. X., 2013, Determination of rock acoustic properties at low frequency: A differential acoustical resonance spectroscopy device and its estimation technique: Geophysical Research Letters, **40**, 2975–2982.

Zhao, J. G., Wang, S. X., Tong, X. L., Yin, H. J., Yuan, D. J., Ma, X. Y., Deng, J. X., and Xiong, B., 2015, Geophysical Journal International, **202**, 1775–1791.

Ma Xiao-Yi received his Ph.D. from China University of Petroleum (Beijing) in 2018. Main research interests are experimental rock physics. Email: ma_xiaoyi@sina.com